

Studying [CII] Emission in Low-mass Galaxies at $z \sim 7$

Kelsey Glazer¹, Maruša Bradač^{1,2}, Ryan L. Sanders^{1,8}, Seiji Fujimoto³, Patricia Bolan¹,
 Andrea Ferrara⁴, Victoria Strait^{5,6}, Tucker Jones¹, Brian C. Lemaux^{1,7}, Livia Vallini⁹,
 Russell Ryan¹⁰

¹Department of Physics and Astronomy, University of California, Davis, 1 Shields Ave, Davis, CA 95616, USA

²University of Ljubljana, Department of Mathematics and Physics, Jadranska ulica 19, SI-1000 Ljubljana, Slovenia

³Department of Astronomy, The University of Texas at Austin, Austin, TX 78712, USA

⁴Scuola Normale Superiore, Piazza dei Cavalieri 7, 50126 Pisa, Italy

⁵Cosmic Dawn Center (DAWN), Denmark

⁶Niels Bohr Institute, University of Copenhagen, Jagtvej 128, DK-2200 Copenhagen N, Denmark

⁷Gemini Observatory, NSF's NOIRLab, 670 N. Aohoku Place, Hilo, Hawai'i, 96720, USA

⁸Department of Physics and Astronomy, University of Kentucky, Lexington, KY 40506, USA

⁹INAF-Osservatorio di Astrofisica e Scienza dello Spazio, via Gobetti 93/3, I-40129, Bologna, Italy

¹⁰Space Telescope Science Institute, 3700 San Martin Drive, Baltimore, MD 21218, USA

Accepted XXX. Received YYY; in original form ZZZ

ABSTRACT

We report on a [CII]_{158 μ m} search using the Atacama Large Millimeter/submillimeter Array (ALMA) on three lensed, confirmed Ly α emitting galaxies at $z \sim 7$. Our targets are ultra-violet (UV) faint systems with stellar masses on the order of $M_* \sim 10^9 M_\odot$. We detect a single [CII] line emission (4σ) from the brightest ($L \sim 2.4 \times 10^{10} L_\odot$) galaxy in our sample, MACS0454-1251. We determine a systemic redshift ($z_{\text{[CII]}} = 6.3151 \pm 0.0005$) for MACS0454-1251 and measure a Ly α velocity offset of $\Delta v \approx 300 \pm 70 \text{ km s}^{-1}$. The remaining two galaxies we detect no [CII] but provide 3σ upper limits on their [CII] line luminosities which we use to investigate the $L_{\text{[CII]}} - \text{SFR}$ relation. Overall our single [CII] detection shows agreement with the relation for local dwarf galaxies. Our [CII] deficient galaxies could potentially be exhibiting low metallicities ($Z < Z_\odot$). Another possible explanation for weaker [CII] emission could be strong feedback from star formation disrupting molecular clouds. We do not detect continuum emission in any of the sources, placing upper limits on their dust masses. Assuming a single dust temperature of $T_d = 35\text{K}$ dust masses (M_{dust}) range from $< 4.8 \times 10^7 M_\odot$ to $2.3 \times 10^8 M_\odot$. Collectively, our results suggest faint reionization era sources could be metal poor and/or could have strong feedback suppressing [CII] emission.

Key words: galaxies:high-redshift – gravitational lensing:strong

1 INTRODUCTION

In the past decade, the Atacama Large Millimeter/submillimeter Array (ALMA) observations of metal fine structure lines such as the [CII]_{158 μ m} line have opened up studies into the epoch of reionization (EoR; $z > 6$) by providing an unobscured view of galaxies. With the advent of the James Webb Space Telescope (JWST), which can also provide a similar a view of non-resonant optical lines (e.g., H α), ALMA observations still provide a complementary view for far infrared (FIR) emission lines. FIR lines hold immense value for EoR studies because they are not affected by dust extinction, in contrast to rest-optical lines accessible with JWST. There have been numerous [CII] detections in UV-bright, high- z ($z > 6$) galaxies (e.g., Willott et al. 2015; Carniani et al. 2017; Laporte et al. 2017; Smit et al. 2018a; Matthee et al. 2019; Harikane et al. 2019; Bakx et al. 2020). However, there are considerably fewer recorded [CII] detections for characteristically faint, $L < L_{z\sim 7}^*$ (where L^* is the characteristic luminosity) EoR galaxies (e.g., Schaerer et al. 2015; Watson et al. 2015; Knudsen et al. 2016; Bradač et al. 2017; Fujimoto et al. 2021; Laporte et al. 2021). Faint galaxies are much more numerous than bright ($L < L_{z\sim 7}^*$) galaxies (e.g. Bouwens et al. 2022; Bolan et al.

2022) and, as such, can be a key driver of reionization. However, this connection has been heavily debated (e.g. Finkelstein et al. 2019; Naidu et al. 2020; Robertson 2022; Endsley et al. 2023). In order to resolve this question, we need to study the physical properties of these fainter primordial systems; this step is key to understanding their role in cosmic reionization.

Here we use [CII] observations to study $z \sim 7$ galaxies. The [CII] line is of particular interest because it predominantly traces the dense neutral gas in photodissociation regions (PDRs, Wolfire et al. 2022) associated with molecular clouds, and the diffuse neutral gas (Wolfire et al. 2003; Hollenbach & Tielens 1999). It is the most luminous line in the FIR band ($\sim 0.1 - 1\%$ of the FIR luminosity, Baier-Soto et al. 2022) and one the strongest emission lines of star-forming galaxies at FIR/radio wavelengths (Carilli & Walter 2013; Stacey et al. 1991, 2010). Additionally, the [CII] line can be used to trace the systemic redshift, and therefore velocity, of the host galaxy because it is optically thin and not affected by dust extinction. When paired with detected Ly α emission, we can estimate interstellar medium (ISM) properties of the galaxy under some assumptions. For instance, we can estimate the amount of neutral gas assuming

the offset stems from $\text{Ly}\alpha$ resonant scattering in ISM gas (Mason et al. 2018).¹ $\text{Ly}\alpha$ photons travelling through neutral ISM scatter more frequently and emerge with a larger Δv compared to photons traveling through less neutral ISM (Yang et al. 2016, 2017; Guaita et al. 2017). Previous observations of $z > 5$ galaxies have typically measured $\Delta v \lesssim 500 \text{ km s}^{-1}$ (Cassata et al. 2020; Carniani et al. 2018a; Pentericci et al. 2016; Bunker et al. 2023; Prieto-Lyon et al. 2023) with the largest $\Delta v \approx 1000 \text{ km s}^{-1}$ recorded by Baier-Soto et al. (2022). Cassata et al. (2020) find that galaxies ($4.4 < z < 6$) with smaller Δv have larger $\text{Ly}\alpha$ rest-frame equivalent widths and $f_{\text{esc}}(\text{Ly}\alpha)$. However, for intrinsically faint systems ($M_{\text{UV}} \gtrsim -20.5$) at $z > 6$, a limited sample size restricts our ability to make robust conclusions (see Endsley et al. 2022 and references therein).

In addition to velocity offsets, we can also measure [CII] line luminosities ($L_{[\text{CII}]}$) and evaluate the empirical [CII] line luminosity to star formation rate ($L_{[\text{CII}]} - \text{SFR}$) relation. This tight relation is well established for a wide range of local galaxy types (e.g., Boselli et al. 2002; De Looze et al. 2011, 2014; Sargsyan et al. 2012; Pineda et al. 2014; Herrera-Camus et al. 2015), but initial [CII] searches in $z > 5$ galaxies revealed lower than expected or missing [CII] emission from "normal" ($\text{SFR} < 100 M_{\odot} \text{ yr}^{-1}$) star-forming galaxies (see Carniani et al. 2020 and references therein). The coined "[CII] deficit" problem brought into question whether or not [CII] could remain a good tracer of SFR at higher- z systems as well as the applicability of the low- z $L_{[\text{CII}]} - \text{SFR}$ relation. Observational studies (e.g., Maiolino et al. 2015; Capak et al. 2015; Knudsen et al. 2016; Matthee et al. 2017; Carniani et al. 2018b; Matthee et al. 2019; Schaerer et al. 2020; Romano et al. 2022) have focused on understanding the $L_{[\text{CII}]} - \text{SFR}$ relation and if there indeed is missing [CII] emission for $z \sim 7$.

Theoretical studies have also extensively modeled the under/undetected [CII] emission (e.g., Vallini et al. 2013, 2015; Olsen et al. 2017; Katz et al. 2017, 2019; Pallottini et al. 2017, 2022; Lupi & Bovino 2020). The analytical approach by Ferrara et al. (2019) concluded that under-luminous [CII] systems can result from a combination of factors: (a) large upward deviations from the Kennicutt-Schmidt relation (corresponding to bursty phases); (b) low metallicity; (c) low gas density, at least for the most extreme sources. These results have been supported by cosmological numerical simulations (Vallini et al. 2015; Pallottini et al. 2019).

As mentioned previously, majority of EoR studies investigating [CII] have targeted UV-bright galaxies, which traditionally have higher SFRs. These larger and brighter galaxies are inherently easier to observe but do not exemplify galaxies at this epoch. Lensing, in our case by foreground galaxy clusters, serves as an excellent way to increase the apparent brightness and size of these fainter systems. In particular, the flux of such objects is increased by a magnification factor μ and resolution improved by $\sqrt{\mu}$. In this paper we report on a [CII] study carried out with ALMA that targeted a set of lensed, sub- L_* galaxies with $\text{SFRs} < 20 M_{\odot} \text{ yr}^{-1}$. The lensed sizes of our galaxies are compact and smaller than the beam sizes of observations. All objects in our sample are spectroscopically confirmed EoR galaxies via detected $\text{Ly}\alpha$ emission. We acknowledge a sample of galaxies all with detected $\text{Ly}\alpha$ emission could potentially bias our results. However, recent results by Bolan et al. in prep find no significant difference in stellar UV properties (e.g. stellar mass, star formation rate, specific star formation rate, UV magnitude, β -slope, age) between $\text{Ly}\alpha$ emitters and non-emitters at $5 < z < 8.2$ in the similar stellar mass range to the one studied here.

The paper is organized as follows. Section 2 explains various ob-

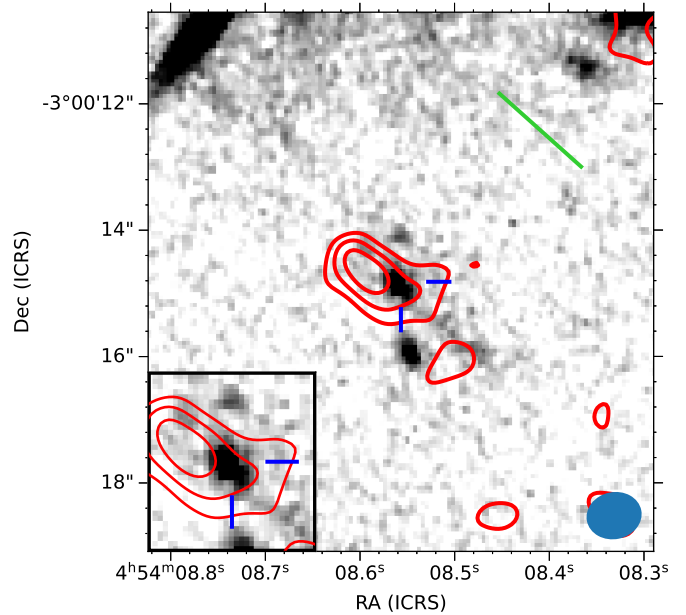


Figure 1. MACS0454-1251 velocity-integrated [CII] line intensity overlaid on a *HST*/WFC3 F160W image. The contours are shown in red and are spaced linearly by intervals of 1σ which range from 2, 3, and 4σ (RMS = 87.1 mJy/beam). The beam size ($0''.88 \times 0''.82$) is given in the bottom right with a $2'' \times 2''$ zoom-in shown in the bottom left. The galaxy is located at an RA and DEC of $04:54:08.56$, $-03:00:14.82$ (UV centroid) with blue cross hairs marking the target in the center. The direction of shear is shown by the green line.

servations used to compile our sample and the specific ALMA data reduction performed on our data. In Section 3 we discuss the measurements and derived properties from the ALMA data as well as the spectral energy density (SED) fitting performed for galaxy property estimates. In Section 4 we analyze and discuss our results with literature findings. In Section 5 we summarize our conclusions. Throughout this paper we assume a Λ CDM concordance cosmology with $\Omega_m = 0.27$, $\Omega_\Lambda = 0.73$ and Hubble constant $H_0 = 73 \text{ km s}^{-1} \text{ Mpc}^{-1}$. Coordinates are given for the epoch J2000.0, magnitudes are in the AB system, and we use the Chabrier (2003) initial mass function (IMF).

2 OBSERVATIONS AND DATA REDUCTION

The lensing galaxy clusters of our sample have been extensively studied in past works. All three clusters have imaging from the *Hubble Space Telescope* (*HST*). The Cluster Lensing and Supernova Survey with Hubble (CLASH, Postman et al. 2012) program observed MACS2129 and RXJ1347. The two CLASH clusters were also spectroscopically observed with The Grism Lens-Amplified Survey from Space (GLASS, Treu et al. 2015) program. MACS0454 was imaged with the *HST*-GO-11591 (PI: Kneib)/GO-9836 (PI: Ellis)/GO-9722 (PI: Ebeling) programs. Additionally, the three clusters were imaged with the *Spitzer* Ultra Faint Survey Program (SURFSUP Bradač et al. 2014) which observed a total of ten lensing clusters. Spectroscopic follow ups using the DEep Imaging Multi-Object Spectrograph (DEIMOS, Faber et al. 2003) and Multi-Object Spectrometer for InfraRed Exploration (MOSFIRE, McLean et al. 2010) instruments on *Keck* confirmed $\text{Ly}\alpha$ emission in the galaxies that

¹ We remind that outflows might also generate comparable velocity offsets.

Table 1. Properties of observed galaxies.

Target ID	$z_{\text{Ly}\alpha}$	μ_{best}^a	Ref ^b	β_{UV}	$EW_{\text{Ly}\alpha}^b$	$M_* \times f_{\mu}^{d,e}$	$\text{SFR}_{\text{SED}} \times f_{\mu}^{d,e}$	$\text{SFR}_{\text{UV}} \times f_{\mu}^{d,f}$	Age ^e	M_{UV}^d	L^g
–	–	–	–	–	Å	$10^9 M_{\odot}$	$M_{\odot} \text{yr}^{-1}$	$M_{\odot} \text{yr}^{-1}$	Myr	mag	L^*
MACS0454-1251	6.323 ± 0.002^h	4.4 ± 0.4	[1]	-1.6 ± 0.2^b	6.8 ± 0.9^c	$5.52_{-1.5}^{+1.6}$	$13.5_{-3.9}^{+4.1}$	8.82 ± 0.15	55_{-29}^{+58}	-20.8 ± 0.1	0.74 ± 0.09
MACS2129-1412	6.846 ± 0.001	$11_{-0.7}^{+0.1}$	[2]	-0.93 ± 0.6^e	60 ± 11	$1.73_{-0.61}^{+4.2}$	$6.93_{-2.4}^{+5.9}$	1.06 ± 0.04	216_{-80}^{+330}	-18.6 ± 0.2	0.10 ± 0.02
RXJ1347-018	7.161 ± 0.001	$21.4_{-1.3}^{+1.7}$	[3]	-1.6 ± 1.0^e	27.2 ± 6.5	$2.49_{-2.0}^{+3.0}$	$7.5_{-5.7}^{+12}$	0.29 ± 0.01	249_{-147}^{+335}	$-17.2 \pm +0.2$	0.03 ± 0.01

^a To use a different magnification factor μ , simply use $f_{\mu} \equiv \mu / \mu_{\text{best}}$, where μ_{best} is the magnification factor we adopt for each object.

^b References for photometry, lens modeling and, Ly α : [1]Huang et al. (2016a), [2] Huang et al. (2016b), [3]Hoag et al. (2019b).

^c Value has been averaged from two night observations: $8.2 \pm 1.4 \text{ \AA}$ (first night) and $5.4 \pm 1.0 \text{ \AA}$ (second night).

^d Values have been corrected for lensing using μ_{best} .

^e Values derived from SED fitting described in Section 3.

^f SFR_{UV} calculated from lens-corrected M_{UV} magnitudes with Eq.1 from Kennicutt (1998a) converted to Chabrier IMF via $0.63 \times \text{SFR}(\text{Salpeter})_{\text{UV}} = \text{SFR}(\text{Chabrier})_{\text{UV}}$.

^g We adopt the characteristic magnitude $M^* = -21.13 \pm 0.08$ from Bouwens et al. (2022).

^h Measured on two different DEIMOS slitmasks at $z = 6.32403$ and $z = 6.32228$ with $\langle z \rangle = 6.3232 \pm 0.0018$. Uncertainty reflects difference between the mask measurements.

make up our sample for this work (Huang et al. 2016a,b; Hoag et al. 2019b).

ALMA observations (Proposal ID: 2019.1.00003.S) were carried out between March of 2020 and April 2021 using ALMA Band 6 with 43 12-m antennae in array configurations C43 – 4 and C43 – 5. The precipitable water vapor (PWV) ranged from 0.5mm to 2.1mm. The spectral setup consisted of one spectral window centered on the expected observed frequency of [CII] $_{158\mu\text{m}}$ estimated from the Ly α redshift. The remaining two spectral windows were used for continuum measurements. The on-source time varied from 20 to 35 minutes per target.

The data was reduced and calibrated with the Common Astronomy Software Applications (CASA) package, version 6.1.1.15 following standard procedures. We reimagined the data with the CASA task TCLEAN, adopting Briggs weighting with ROBUST=2.0 (effectively natural weighting) and adding UVTAPER=0''.6. We adopt the taper = 0''.6, given the typical [CII] effective radius of $\sim 2\text{kpc}$ at $z \sim 4 - 6$ (Fujimoto et al. 2020) which corresponds to 0''.3. The angular resolution for each object is equal to their respective beam sizes which increased globally by a factor of ~ 4 when the taper was applied. The RMS also increased when the taper was applied by a factor of ~ 1.56 (MACS0454-1251), ~ 1.36 (MACS2129-1412), and ~ 1.13 (RXJ1347-018) respectively. The final beam sizes and RMS values are quoted in the captions of the contour figures. All three targets were unresolved in their final data products and were spectrally binned into 25-km s $^{-1}$ velocity channels. To ensure positional accuracy, we astrometrically calibrated *HST* reference images to GAIA DR2 when comparing [CII] to UV emission. Continuum maps were made with all spectral windows.

3 MEASUREMENTS AND DERIVED PROPERTIES

We observed three highly magnified ($\mu \sim 4 - 20$) Lyman alpha emitting (LAEs) galaxies with ALMA at $z_{\text{Ly}\alpha} = 6.323 \pm 0.003$ (MACS0454-1251), 6.846 ± 0.001 (MACS2129-1412), and 7.161 ± 0.001 (RXJ1347-018). We report a single [CII] detection (4σ , Fig 1) from MACS0454-1251. We extracted the spectrum over an extended

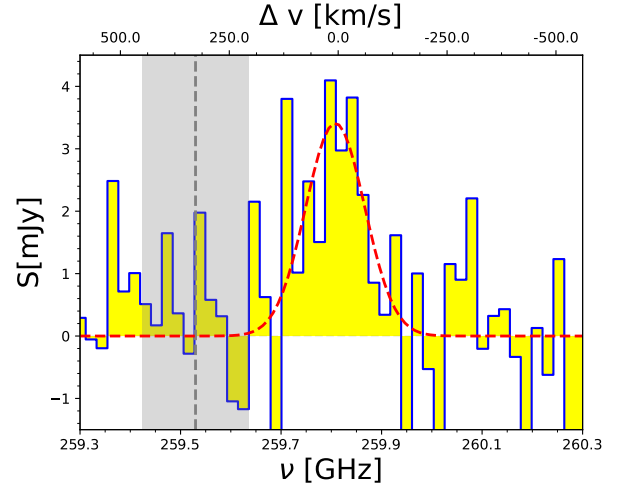


Figure 2. Extracted spectrum showing the detected [CII] emission. Flux (left axis) shown as a function of frequency (bottom axis) and velocity (top axis). Red dashed line represents the best fit Gaussian and grey dashed line represents Lyman- α redshift with boxed 1σ uncertainty.

elliptical aperture (semi-axes: $\sim 1.''5 \times 0.''5$, pitch angle: $\sim 35^\circ$) to account of the slightly oblong shape in the [CII] contours of the moment0 map (see Fig 1). We note that the SNR was slightly improved when the uvtaper was optimized to the elliptical morphology of the source. We fit a Gaussian (see Fig 2) to estimate the peak line flux $S_{\text{line}} = 3.7 \pm 0.9\text{mJy}$. We calculate the integrated line flux ($S_{\text{line,g}} \Delta v$) as $0.64 \pm 0.15\text{Jykm s}^{-1}$ with a FWHM of $163 \pm 46\text{km s}^{-1}$. We determine the systemic redshift $z_{[\text{CII}]} = 6.315 \pm 0.001$ which is in close agreement with the redshift found via Ly α ($z_{\text{spec}} = 6.323$). The calculated [CII] line luminosity (eq.18, Casey et al. 2014) is $L_{[\text{CII}]} = 1.5_{-0.4}^{+0.5} \times 10^8 L_{\odot}$ and find a velocity offset (the difference between Ly α and [CII]: $v_{\text{Ly}\alpha} - v_{[\text{CII}]}$) $\Delta v = 320 \pm 70\text{km s}^{-1}$. We estimate the physical size of the emission by fitting a 2D Gaussian and deconvolving the clean beam from the map. The beam-deconvolved size of the major and minor axes are $1.37'' \pm 0.18''$ and $0.41'' \pm 0.21''$.

Table 2. Results from ALMA.

Target ID	$z_{\text{[CII]}}$	S_{line} (mJy)	FWHM (kms $^{-1}$)	$S_{\text{line}}\Delta\nu$ (Jykm s $^{-1}$)	$L_{\text{[CII]}} \times f_{\mu}$ ($\times 10^8 L_{\odot}$)	Continuum ^a (μ Jy)	$L_{\text{FIR}} \times f_{\mu}^{a,b}$ ($\times 10^{10} L_{\odot}$)	$\text{SFR}_{\text{FIR}}^{a,b,c}$ $M_{\odot}\text{yr}^{-1}$	$M_{\text{dust}}^{a,c}$ $\times 10^8 M_{\odot}$
MACS0454-1251	6.3151 ± 0.0005	$3.7_{-0.9}^{+0.9}$	163 ± 46	$0.64 \pm +0.15$	$1.5_{-0.4}^{+0.5}$	< 1380	< 32	< 35	< 2.3
MACS2129-1412	–	–	–	–	< 0.043	< 18.3	< 0.19	< 0.21	< 0.93
RXJ1347-018	–	–	–	–	< 0.062	< 47.0	< 1.1	< 1.2	< 0.48

^a All limits are 3σ

^b Calculated from Kennicutt (1998b) Eq.3, which was converted to Chabrier IMF via $0.63 \times \text{SFR}(\text{Salpeter})_{\text{FIR}} = \text{SFR}(\text{Chabrier})_{\text{FIR}}$

^c Assumed $T_{\text{d}} = 35\text{K}$.

This corresponds to a physical size of $\sim 3.6 \pm 0.5\text{kpc} \times 1.1 \pm 0.6\text{kpc}$ after dividing by $\sqrt{\mu}$ to account for lensing. We divide the FWHM by 2.0 to compare with effective radii found in a previous study (Fujimoto et al. 2020) at $z = 4 - 6$. The resulting [CII] size of our semi-major axis ($\sim 1.8 \pm 0.3\text{kpc}$) is consistent with the $\sim 2 - 3\text{kpc}$ sizes reported in Fujimoto et al. (2020).

The remaining two galaxies, MACS2129-1412 and RXJ1347-018, yielded non-detections for [CII] emission (see Fig 3). Because their intrinsic [CII] line widths are unknown, we estimate their $L_{\text{[CII]}}$ (3σ) upper limits by integrating over the same width of channels (9 channels, 225km s^{-1}) as was done in MACS0454-1251. In the absence of known systemic redshifts, we use $\text{Ly}\alpha$ redshifts to predict expected [CII] emitting frequency of each object². The RMS uncertainty was calculated using the 1σ intensity value extracted from a $0.''5$ aperture centered to the HST imaging centroid of the target. We list the calculated $L_{\text{[CII]}}$ (3σ) upper limits in Table 2.

We constructed a continuum map for MACS0454-1251 from all four spectral windows (SPWs), masking out the channels expected to contain [CII] emission. As seen in Fig 2, the [CII] line of MACS0454-1254 appears to be extended over roughly nine channels which corresponds to a width of 225km s^{-1} . All nine channels were masked when producing the final continuum map from which we derived an upper limit on L_{FIR} . We assume a wavelength range of $8 - 1000\mu\text{m}$ for L_{FIR} calculation. For the remaining non-detection galaxies, we constructed continuum maps in the same manner excluding nine channels centered on the central frequency. To estimate L_{FIR} , we used a grey-body spectral energy distribution model (Casey 2012), assuming a spectral index of $\beta = 1.5$. In the absence of multi-band observations, we assumed a uniform dust temperature ($T_{\text{d}} = 35\text{K}$) across all three objects and estimated $3\sigma L_{\text{FIR}}$ which is recorded in table 2. In similar studies where dust continuum was not detected (Fujimoto et al. 2022; Fudamoto et al. 2023; Witstok et al. 2022), assumed dust temperatures varied $T_{\text{d}} = 40 - 60\text{K}$. Other studies on mostly massive galaxies (Fujimoto et al. 2021; Bakx et al. 2021; Algera et al. 2024; Witstok et al. 2022; Sommovigo et al. 2022) also have a sizeable range on $T_{\text{d}} = 32 - 59\text{K}$ with considerable error at low and high ends (note that employing single band techniques to estimate dust temperature was shown to overestimate temperatures by $\sim 15\text{K}$). Because L_{FIR} and M_{dust} are directly related to the assumed T_{d} , assuming a lower T_{d} sets a lower limit on L_{FIR} and a conservative upper limit on M_{dust} .

Because we do not detect continuum in all three galaxies, we provide SFR_{FIR} and M_{dust} limits in Table 2. We estimated SFR_{FIR}

using eq.3 from Kennicutt (1998b) and converted from Salpeter IMF to Chabrier IMF. We assumed a dust mass absorption coefficient of $\kappa = \kappa_0(\nu/\nu_0)^{\beta_{\text{d}}}$, where $\kappa_0 = 0.232\text{m}^2\text{kg}^{-1}$ at $\nu_0 = 250\mu\text{m}$ (Draine 2003; Bianchi 2013).

To estimate age and stellar mass (M_{stellar}) of the sample, we use Bayesian Analysis of Galaxies for Physical Inference and Parameter ESTimation (BAGPIPES, Carnall et al. 2018). BAGPIPES fits physical parameters using the MultiNest sampling algorithm (Feroz & Hobson 2008; Feroz et al. 2009). We use the default set of stellar population templates from Bruzual and Charlot (Bruzual & Charlot 2003, BC03). The SED fitting is done assuming the Kroupa (2001) IMF which we convert to Chabrier (2003), a metallicity of $0.02Z_{\odot}$, the Calzetti dust law (Calzetti et al. 2000), and a constant star formation history. We allow dust extinction to range from $A_{\text{v}} = 0 - 3$ magnitudes. The M_{stellar} values reflected in Table 1 have been converted to Chabrier IMF via conversion factor 0.923. We take the general prescription for the fitting from Strait et al. (2020). See Bolan et al. in prep. for more information on the SED fitting.

4 RESULTS

4.1 Velocity and Spatial Offset

Observational studies have used [CII] emission as a tracer of systemic velocities (e.g Pentericci et al. 2016; Matthee et al. 2019). Using the peak [CII] emission from the extracted spectrum of MACS0454-1251, we find $\Delta\nu_{\text{Ly}\alpha - \text{[CII]}} \approx 320 \pm 70\text{km s}^{-1}$. This is shown in Fig 2 where the velocity axis is centered on the [CII] emission and the grey dashed line represents $\text{Ly}\alpha$. The magnitude of the offset falls within literature ranges quoted for $z = 2 \sim 3$ (Erb et al. 2014) and high- z galaxies (e.g., Cassata et al. 2020; Endsley et al. 2022).

The spectrum shows a clear redshift of $\text{Ly}\alpha$ emission. Given the resonant nature of $\text{Ly}\alpha$, revealing the direct cause of the offset is both a complex and active place of research. Redshifted $\text{Ly}\alpha$ could indicate scattered emission from outflowing (or expanding) gas from the galaxy. Outflows may originate from strong star formation feedback which could reduce the covering fraction of neutral gas in the ISM and boost $\text{Ly}\alpha$ escape (Jones et al. 2013; Trainor et al. 2015; Leethochawalit et al. 2016). $\text{Ly}\alpha$ could also be redshifted by neutral hydrogen inside a galaxy's ISM, where the emerging $\Delta\nu$ would be a proxy for the column density of neutral hydrogen (Yang et al. 2016, 2017; Guaita et al. 2017). Additionally, the model put forth by Mason et al. (2018) used $\Delta\nu$ as a way to measure the intergalactic medium (IGM) neutral fraction. A more neutral IGM will scatter $\text{Ly}\alpha$ photons more causing $\text{Ly}\alpha$ to emerge at a higher $\Delta\nu$ relative to systemic.

It is not uncommon for $z > 5$ galaxies to have [CII] emission

² This assumes there is no velocity offset between $\text{Ly}\alpha$ and [CII] emission for these two galaxies

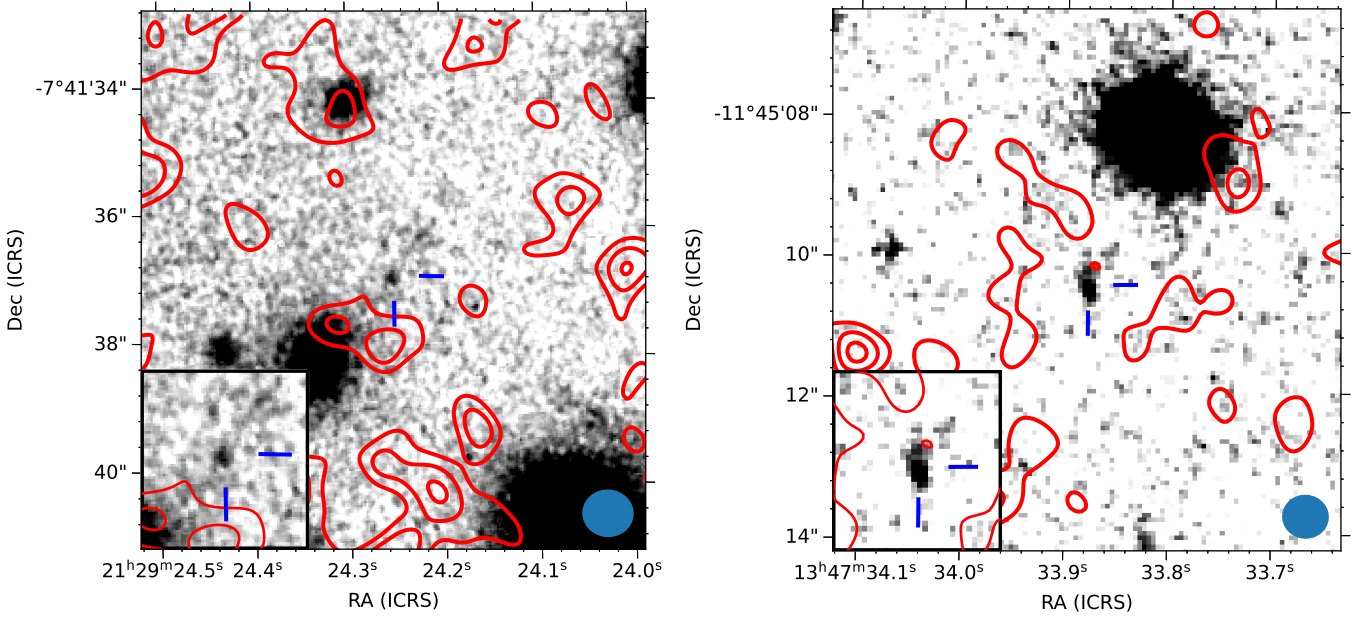


Figure 3. MACS2129-1412 (left) and RXJ1347-018 (right) velocity-integrated [CII] line intensity overlaid on *HST*/WFC3 F160W image. The contours are shown in red and linearly spaced at 1σ intervals from $1 - 4\sigma$ (RMS = 15.3mJy/beam and 34.8mJy/beam respectively). The beam is given in the bottom right ($0''.82 \times 0''.76$ for MACS2129-1412, $0''.66 \times 0''.62$ for RXJ1347-018) with a $2'' \times 2''$ zoom-in shown in the bottom left. Respective RAs and DECJs (for UV emission) of these two galaxies are 21:29:24.23, $-07:414:35.96$ (MACS2129-1412) and 13:47:33.90, $-11:45:09.40$ (RXJ1347-018) with the objects outlined by blue cross hairs on the *HST* images.

tracing the systemic redshift of the galaxy but spatially offset from the UV component (Maiolino et al. 2015; Willott et al. 2015; Capak et al. 2015; Carniani et al. 2017, 2018b,a; Jones et al. 2017; Matthee et al. 2019; Fujimoto et al. 2022). In fact, spatial offsets between Ly α and UV have also been found at $z > 5$ (Hoag et al. 2019a; Lemaux et al. 2021). Carniani et al. (2018a) shows that most of the [CII] spatial offsets are indeed physically motivated but further observations are needed to understand the mechanisms causing the offsets. Recently, Fujimoto et al. (2022) was able to determine the necessity of past outflow activity in a galaxy at $z \sim 8.5$ based on dual observations with ALMA and JWST.

We roughly estimate the [CII]-UV spatial offset in MACS0454-1251 using the brightest pixels found in the [CII] moment0 map and the centroid of the *HST* rest-UV image. The lensed spatial offset is $\sim 0''.5$ which is greater than the ALMA astrometric accuracy of $\sim 0''.08$ ³. Taking into account the magnification, we estimate the lens-corrected offset to be $\sim 1.4\text{kpc}$ ⁴. The offset could be physically associated with intrinsic ISM properties (e.g. different distribution in the ionized vs neutral gas phase). A possible explanation for the spatial offset could also be the ejection of material by galactic outflows or galaxy mergers (e.g., Maiolino et al. 2015; Vallini et al. 2015; Pallottini et al. 2017; Katz et al. 2017; Gallerani et al. 2018; Kohandel et al. 2019).

³ Calculated from ALMA technical handbook <https://almascience.nrao.edu/documents-and-tools/cycle10/alma-technical-handbook>.

⁴ For isotropic lensing distortion, we spatially scale with $1/\sqrt{\mu}$

4.2 $L_{[\text{CII}]}$ – SFR Relation

In Fig 4 we show the $L_{[\text{CII}]}$ – SFR_{UV} relation for our galaxies (stars) alongside available $z > 6$ observations from the literature. The reported SFR_{UV} values for our objects can be found in Table 1 along with SFR_{SED} values that were derived through SED fitting described in Section 3. SFR_{UV} is calculated assuming no dust attenuation and therefore should be considered a lower limit as it does not include obscured star formation. We also recognize that in the event of a more top heavy IMF (i.e., the median of the mass-to-light ratio of stars being born decreases), SFR_{UV} would be an overestimate assuming constant dust properties.

Our single [CII] detection, MACS0454-1251, falls within the 1σ scatter of the De Looze et al. (2014) relation for dwarf (~ 0.2 dex below). We note, however, MACS0454-1251 is the most UV luminous galaxy ($L = 0.74L^*$) in our sample. The detection is also consistent with the C1 model put forth by the Vallini et al. (2015) simulations which corresponds to a galaxy with constant solar metallicity. If we compare this to our non-detections, the upper limit set by RXJ1347-018 also is consistent with the De Looze et al. (2014) relation; having a scatter of ~ 0.3 dex from the average. The upper limit set by MACS2129-1412 is not consistent with the De Looze et al. (2014) relation, falling ~ 0.6 dex from the dwarf galaxies. The one displayed Vallini et al. (2015) model it could possibly support is the C005 model which represents a galaxy with a constant metallicity of $Z = 0.05Z_{\odot}$.

The analysis presented here focuses on the SFR_{UV} component, but SFR_{SED} as well as upper limits on SFR_{FIR} are provided for completeness. The SFR_{UV}/SFR_{FIR} limits are not very constraining for our galaxies given we only have upper limits on SFR_{FIR} making us unable to exclude any model considered in this

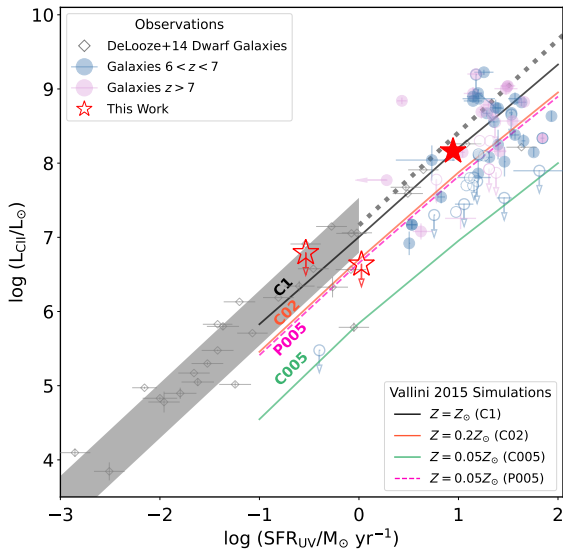


Figure 4. A plot of $L_{[\text{CII}]}$ vs. SFR_{UV} relation for our study (red stars) and literature. The blue ($z > 6$) and purple ($z > 7$) circles show previous studies Willott et al. (2015); Maiolino et al. (2015); Knudsen et al. (2016); Pentericci et al. (2016); Matthee et al. (2017); Bradač et al. (2017); Carniani et al. (2018a); Smit et al. (2018b); Hashimoto et al. (2018); Matthee et al. (2019); Schouws et al. (2022); Harikane et al. (2020); Fujimoto et al. (2021); Molyneux et al. (2022); Schaerer et al. (2015); Inoue et al. (2016); Carniani et al. (2020); Watson et al. (2015); Wong et al. (2022); Katz et al. (2017); Bakx et al. (2020); Bowler et al. (2018); Hashimoto et al. (2019); Fujimoto et al. (2022); Heintz et al. (2023); Ferrara et al. (2022); Sommovigo et al. (2022); Valentino et al. (2022). Upper limits are denoted by open markers. The lines represent the results from Vallini et al. (2015) with black $Z = Z_{\odot}$ (C1), orange $Z = 0.2Z_{\odot}$ (CO2), and green $Z = 0.05Z_{\odot}$ (CO05) representing a constant metallicity. The magenta dashed line (P005) represents a density-dependent metallicity of $Z = 0.05Z_{\odot}$. The best-fit dwarf relation from De Looze et al. (2014) is shown in gray with measurements as open gray diamonds. Above $\text{SFR} = 1M_{\odot}/\text{yr}$, the relation is shown as a gray dotted line with 1σ scatter to emphasize that only a few galaxies constrain the higher $L_{[\text{CII}]}/\text{SFR}$ regime.

work. We do note the $\text{SFR}_{\text{FIR}} < \text{SFR}_{\text{UV}}$ for MACS2129-1412 shows $\text{SFR}_{\text{FIR}} < \text{SFR}_{\text{UV}}$. For the M_{dust}/M_{*} , all three of our galaxies showed limits $\log M_{\text{dust}}/\log M_{*} \lesssim 0.8$. Our limits are consistent within 1σ of the overall values reported in Sommovigo et al. (2022) ($\log M_{\text{dust}}/\log M_{*} \approx 0.74-0.81$) who studied 13 higher-mass galaxies at $z \sim 7$. Our limits are also consistent with the dust build up reported in Pozzi et al. (2021).

We also advise caution when drawing comparisons between our objects and the dwarf relation in De Looze et al. (2014). As shown in Fig 4, majority of dwarf galaxies (gray diamonds) used to make the best-fit relation (gray dotted line) are much lower luminosity systems than those reported in this paper as well as literature. Above $\text{SFR} \sim 1M_{\odot}\text{yr}^{-1}$ the dwarf relation is less constrained, being driven by only a handful of dwarf galaxies.

The solar and sub-solar metallicity models by Vallini et al. (2015) provide a unique view on the metal content of our galaxies. The possibility of a sub-solar metallicities is not surprising for our three low-mass galaxies and aligns with recent work (Curti et al. 2023; Nakajima et al. 2023). Although Curti et al. (2023) probed a moderately lower mass range than our sample, they found their $z > 6$ galaxies exhibiting sub-solar metallicities ($Z < Z_{\odot}$), with a scaling

relation drawn near $\sim 0.1Z_{\odot}$. A more comparable study by Nakajima et al. (2023) reported $Z < Z_{\odot}$ for a sub-sample of galaxies ranging from $z = 6 - 10$ with a somewhat larger range of masses. While we do not have the observations to determine the true metallicities of our sample, a low metallicity could explain the absence of [CII] in our non-detections and would not contradict their respective upper limits. Another possible reason for the lack of detected [CII] emission could be negative feedback disrupting molecular clouds (MCs, Vallini et al. 2015). For example, [CII] emission predominately originates from PDRs. Negative feedback disrupting MCs would reduce the PDR layer at the edge of the MC where most of the [CII] emission comes from. Additionally, we know stellar feedback is efficient in galaxy centers, places where there is very active star formation. In fact, studies done at lower- z have supported a connection between feedback efficiency and SFR surface density (e.g., Hayward & Hopkins 2016; Heckman et al. 2011). Since high- z galaxies are more compact than local analogs, this would also support negative feedback suppressing [CII] emission at the systemic redshift of the galaxy.

5 CONCLUSIONS

We present new ALMA observations investigating [CII] $158\mu\text{m}$ line emission in three lensed galaxies at $z > 6$. We find a 4σ [CII] detection in our most luminous galaxy ($L \sim 0.7L_{*}$) MACS0454-1251 and calculate the systemic redshift to be $z_{[\text{CII}]} = 6.3151 \pm 0.0005$. We measure a $\Delta v = 320 \pm 20\text{km s}^{-1}$ and calculate $L_{[\text{CII}]} = 1.5_{-0.4}^{+0.5} \times 10^8 L_{\odot}$. For the remaining two galaxies we do not detect [CII] emission but provide 3σ upper limits for their $L_{[\text{CII}]}$. Our main findings are:

(i) MACS0454-1251 exhibits both a velocity and a spatial offset between ALMA [CII] and rest-frame HST UV emission. The spatial offset is larger than the the ALMA astrometric uncertainty which could mean the offset is physically motivated by intrinsic ISM properties.

(ii) Feedback is a very important process in both the emission of [CII] and $\text{Ly}\alpha$. On one hand, strong feedback can suppress [CII] emission by disrupting MCs (Vallini et al. 2015). On the other hand strong feedback from star formation can drive outflows which redshifts the $\text{Ly}\alpha$ line. A possibility that puts together the spatial offset and the [CII] deficit is that feedback destroys the emitting MCs at the center, allowing only displaced MCs to contribute to the [CII] emission.

(iii) Our single [CII] detection in MACS0454-1251 falls within the 1σ scatter of the De Looze et al. (2014) $L_{[\text{CII}]} - \text{SFR}$ relations. As such, it would support with the applicability of the $L_{[\text{CII}]} - \text{SFR}$ relation put forth by De Looze et al. (2014) for $z > 6$ galaxies. That being said, the upper limits set by our RXJ1347-018 and MACS2129-1412, would argue an inconclusive result, especially with the 3σ upper limit of MACS2129-1412 still falling well below De Looze et al. (2014). In general, more observations of low-mass, UV faint galaxies are needed in order to break this degeneracy.

(iv) Low metallicity is a possible justification for fainter galaxies falling below the De Looze et al. (2014) $L_{[\text{CII}]} - \text{SFR}$ relation (Vallini et al. 2013; Ferrara et al. 2019). Based on recent work (Curti et al. 2023), we would expect lower mass, ($M_{\text{stellar}} \lesssim 10^{9.5}$) galaxies at $z > 6$ to exhibit sub-solar metallicities. A possible scenario for [CII] deficient systems with very low metallicity is powerful feedback; involving the destruction of star forming sites occurring during bursty evolutionary phases in relatively chemically unevolved systems (Vallini et al. 2015; Ferrara et al. 2019).

ACKNOWLEDGEMENTS

We acknowledge support from the program HST-GO-16667, provided through a grant from the STScI under NASA contract NASS-26555. MB also acknowledges support from the ERC Advanced Grant FIRSTLIGHT and Slovenian national research agency ARRS through grants N1-0238 and P1-0188. RLS acknowledges support provided by NASA through the NASA Hubble Fellowship grant #HST-HF2-51469.001-A awarded by the Space Telescope Science Institute, which is operated by the Association of Universities for Research in Astronomy, Incorporated, under NASA contract NASS-26555. AF acknowledges support from the ERC Advanced Grant INTERSTELLAR H2020/740120.

DATA AVAILABILITY

The original data used in the work can be found and downloaded from the ALMA archive <https://almascience.nrao.edu> using the science project ID: 2019.1.00003.S. The reduced data generated in this research will be shared on reasonable request to the corresponding author.

REFERENCES

- Algera H. S. B., et al., 2024, *MNRAS*, **527**, 6867
- Baier-Soto R., Herrera-Camus R., Förster Schreiber N. M., Contursi A., Genzel R., Lutz D., Tacconi L., 2022, *A&A*, **664**, L5
- Bakx T. J. L. C., et al., 2020, *MNRAS*, **493**, 4294
- Bakx T. J. L. C., et al., 2021, *MNRAS*, **508**, L58
- Bianchi S., 2013, *A&A*, **552**, A89
- Bolan P., et al., 2022, *MNRAS*, **517**, 3263
- Boselli A., Gavazzi G., Lequeux J., Pierini D., 2002, *A&A*, **385**, 454
- Bouwens R. J., Illingworth G., Ellis R. S., Oesch P., Stefanon M., 2022, *ApJ*, **940**, 55
- Bowler R. A. A., Bourne N., Dunlop J. S., McLure R. J., McLeod D. J., 2018, *MNRAS*, **481**, 1631
- Bradač M., et al., 2014, *ApJ*, **785**, 108
- Bradač M., et al., 2017, *The Astrophysical Journal*, **836**, L2
- Bruzual G., Charlot S., 2003, *MNRAS*, **344**, 1000
- Bunker A. J., et al., 2023, *arXiv e-prints*, p. [arXiv:2302.07256](https://arxiv.org/abs/2302.07256)
- Calzetti D., Armus L., Bohlin R. C., Kinney A. L., Koornneef J., Storchi-Bergmann T., 2000, *ApJ*, **533**, 682
- Capak P. L., et al., 2015, *Nature*, **522**, 455
- Carilli C., Walter F., 2013, *Annual Review of Astronomy and Astrophysics*, **51**, 105
- Carnall A. C., McLure R. J., Dunlop J. S., Davé R., 2018, *MNRAS*, **480**, 4379
- Carniani S., et al., 2017, *A&A*, **605**, A42
- Carniani S., et al., 2018a, *MNRAS*, **478**, 1170
- Carniani S., Maiolino R., Smit R., Amorín R., 2018b, *ApJ*, **854**, L7
- Carniani S., et al., 2020, *MNRAS*, **499**, 5136
- Casey C. M., 2012, *MNRAS*, **425**, 3094
- Casey C. M., Narayanan D., Cooray A., 2014, *Phys. Rep.*, **541**, 45
- Cassata P., et al., 2020, *A&A*, **643**, A6
- Chabrier G., 2003, *PASP*, **115**, 763
- Curti M., et al., 2023, *arXiv e-prints*, p. [arXiv:2304.08516](https://arxiv.org/abs/2304.08516)
- De Looze I., Baes M., Bendo G. J., Cortese L., Fritz J., 2011, *MNRAS*, **416**, 2712
- De Looze I., et al., 2014, *A&A*, **568**, A62
- Draine B. T., 2003, *ARA&A*, **41**, 241
- Endsley R., et al., 2022, *MNRAS*, **517**, 5642
- Endsley R., Stark D. P., Whitler L., Topping M. W., Chen Z., Plat A., Chisholm J., Charlot S., 2023, *MNRAS*, **524**, 2312
- Erb D. K., et al., 2014, *ApJ*, **795**, 33
- Faber S. M., et al., 2003, in Iye M., Moorwood A. F. M., eds, *Society of Photo-Optical Instrumentation Engineers (SPIE) Conference Series Vol. 4841, Instrument Design and Performance for Optical/Infrared Ground-based Telescopes*. pp 1657–1669, [doi:10.1117/12.460346](https://doi.org/10.1117/12.460346)
- Feroz F., Hobson M. P., 2008, *MNRAS*, **384**, 449
- Feroz F., Hobson M. P., Bridges M., 2009, *MNRAS*, **398**, 1601
- Ferrara A., Vallini L., Pallottini A., Gallerani S., Carniani S., Kohandel M., Decataldo D., Behrens C., 2019, *MNRAS*, **489**, 1
- Ferrara A., et al., 2022, *MNRAS*, **512**, 58
- Finkelstein S. L., et al., 2019, *ApJ*, **879**, 36
- Fudamoto Y., et al., 2023, *arXiv e-prints*, p. [arXiv:2303.07513](https://arxiv.org/abs/2303.07513)
- Fujimoto S., et al., 2020, *ApJ*, **900**, 1
- Fujimoto S., et al., 2021, *The Astrophysical Journal*, **911**, 99
- Fujimoto S., et al., 2022, *arXiv e-prints*, p. [arXiv:2212.06863](https://arxiv.org/abs/2212.06863)
- Gallerani S., Pallottini A., Feruglio C., Ferrara A., Maiolino R., Vallini L., Riechers D. A., Pavesi R., 2018, *MNRAS*, **473**, 1909
- Guaita L., et al., 2017, *A&A*, **606**, A19
- Harikane Y., et al., 2019, *ApJ*, **883**, 142
- Harikane Y., et al., 2020, *The Astrophysical Journal*, **896**, 93
- Hashimoto T., et al., 2018, *Nature*, **557**, 392
- Hashimoto T., et al., 2019, *PASJ*, **71**, 71
- Hayward C. C., Hopkins P. F., 2016, *Monthly Notices of the Royal Astronomical Society*, **465**, 1682
- Heckman T. M., et al., 2011, *ApJ*, **730**, 5
- Heintz K. E., et al., 2023, *ApJ*, **944**, L30
- Herrera-Camus R., et al., 2015, *ApJ*, **800**, 1
- Hoag A., et al., 2019a, *MNRAS*, **488**, 706
- Hoag A., et al., 2019b, *ApJ*, **878**, 12
- Hollenbach D. J., Tielens A. G. G. M., 1999, *Reviews of Modern Physics*, **71**, 173
- Huang K.-H., et al., 2016a, *ApJ*, **817**, 11
- Huang K.-H., et al., 2016b, *ApJ*, **823**, L14
- Inoue A. K., et al., 2016, *Science*, **352**, 1559
- Jones T. A., Ellis R. S., Schenker M. A., Stark D. P., 2013, *ApJ*, **779**, 52
- Jones G. C., Willott C. J., Carilli C. L., Ferrara A., Wang R., Wagg J., 2017, *The Astrophysical Journal*, **845**, 175
- Katz H., Kimm T., Sijacki D., Haehnelt M. G., 2017, *MNRAS*, **468**, 4831
- Katz H., et al., 2019, *MNRAS*, **487**, 5902
- Kennicutt J., 1998a, *Annual Review of Astronomy and Astrophysics*, **36**, 189
- Kennicutt Robert C. J., 1998b, *ApJ*, **498**, 541
- Knudsen K. K., Richard J., Kneib J.-P., Jauzac M., Clément B., Drouart G., Egami E., Lindroos L., 2016, *MNRAS*, **462**, L6
- Kohandel M., Pallottini A., Ferrara A., Zanella A., Behrens C., Carniani S., Gallerani S., Vallini L., 2019, *MNRAS*, **487**, 3007
- Kroupa P., 2001, *MNRAS*, **322**, 231
- Laporte N., Nakajima K., Ellis R. S., Zitrin A., Stark D. P., Mainali R., Roberts-Borsani G. W., 2017, *ApJ*, **851**, 40
- Laporte N., et al., 2021, *MNRAS*, **505**, 4838
- Leethochawalit N., Jones T. A., Ellis R. S., Stark D. P., Zitrin A., 2016, *ApJ*, **831**, 152
- Lemaux B. C., et al., 2021, *MNRAS*, **504**, 3662
- Lupi A., Bovino S., 2020, *MNRAS*, **492**, 2818
- Maiolino R., et al., 2015, *MNRAS*, **452**, 54
- Mason C. A., Treu T., Dijkstra M., Mesinger A., Trenti M., Pentericci L., de Barros S., Vanzella E., 2018, *ApJ*, **856**, 2
- Matthee J., et al., 2017, *The Astrophysical Journal*, **851**, 145
- Matthee J., et al., 2019, *ApJ*, **881**, 124
- McLean I. S., et al., 2010, in McLean I. S., Ramsay S. K., Takami H., eds, *Society of Photo-Optical Instrumentation Engineers (SPIE) Conference Series Vol. 7735, Ground-based and Airborne Instrumentation for Astronomy III*. p. 77351E, [doi:10.1117/12.856715](https://doi.org/10.1117/12.856715)
- Molyneux S. J., et al., 2022, *MNRAS*, **512**, 535
- Naidu R. P., Tacchella S., Mason C. A., Bose S., Oesch P. A., Conroy C., 2020, *ApJ*, **892**, 109
- Nakajima K., Ouchi M., Isobe Y., Harikane Y., Zhang Y., Ono Y., Umeda H., Oguri M., 2023, *ApJS*, **269**, 33
- Olsen K., Greve T. R., Narayanan D., Thompson R., Davé R., Niebla Rios L., Stawinski S., 2017, *ApJ*, **846**, 105

- Pallottini A., Ferrara A., Gallerani S., Vallini L., Maiolino R., Salvadori S., 2017, *MNRAS*, **465**, 2540
- Pallottini A., et al., 2019, *MNRAS*, **487**, 1689
- Pallottini A., et al., 2022, *MNRAS*, **513**, 5621
- Pentericci L., et al., 2016, *The Astrophysical Journal*, **829**, L11
- Pineda J. L., Langer W. D., Goldsmith P. F., 2014, *A&A*, **570**, A121
- Postman M., et al., 2012, *ApJS*, **199**, 25
- Pozzi F., et al., 2021, *A&A*, **653**, A84
- Prieto-Lyon G., et al., 2023, *arXiv e-prints*, p. arXiv:2304.02666
- Robertson B. E., 2022, *ARA&A*, **60**, 121
- Romano M., et al., 2022, *A&A*, **660**, A14
- Sargsyan L., et al., 2012, *ApJ*, **755**, 171
- Schaerer D., Boone F., Zamojski M., Staguhn J., Dessauges-Zavadsky M., Finkelstein S., Combes F., 2015, *A&A*, **574**, A19
- Schaerer D., et al., 2020, *A&A*, **643**, A3
- Schouws S., et al., 2022, *arXiv e-prints*, p. arXiv:2202.04080
- Smit R., et al., 2018b, *Nature*, **553**, 178
- Smit R., et al., 2018a, *Nature*, **553**, 178
- Sommovigo L., et al., 2022, *MNRAS*, **513**, 3122
- Stacey G. J., Geis N., Genzel R., Lugten J. B., Poglitsch A., Sternberg A., Townes C. H., 1991, *The Astrophysical Journal*, **373**, 423
- Stacey G. J., Hailey-Dunsheath S., Ferkinhoff C., Nikola T., Parshley S. C., Benford D. J., Staguhn J. G., Fiolet N., 2010, *The Astrophysical Journal*, **724**, 957
- Strait V., et al., 2020, *ApJ*, **888**, 124
- Trainor R. F., Steidel C. C., Strom A. L., Rudie G. C., 2015, *ApJ*, **809**, 89
- Treu T., et al., 2015, *ApJ*, **812**, 114
- Valentino F., et al., 2022, *ApJ*, **929**, L9
- Vallini L., Gallerani S., Ferrara A., Baek S., 2013, *MNRAS*, **433**, 1567
- Vallini L., Gallerani S., Ferrara A., Pallottini A., Yue B., 2015, *ApJ*, **813**, 36
- Watson D., Christensen L., Knudsen K. K., Richard J., Gallazzi A., Michałowski M. J., 2015, *Nature*, **519**, 327
- Willott C. J., Carilli C. L., Wagg J., Wang R., 2015, *ApJ*, **807**, 180
- Witstok J., et al., 2022, *MNRAS*, **515**, 1751
- Wolfire M. G., McKee C. F., Hollenbach D., Tielens A. G. G. M., 2003, *ApJ*, **587**, 278
- Wolfire M. G., Vallini L., Chevance M., 2022, *ARA&A*, **60**, 247
- Wong Y. H. V., et al., 2022, *arXiv e-prints*, p. arXiv:2202.13613
- Yang H., Malhotra S., Gronke M., Rhoads J. E., Dijkstra M., Jaskot A., Zheng Z., Wang J., 2016, *ApJ*, **820**, 130
- Yang H., et al., 2017, *ApJ*, **844**, 171

This paper has been typeset from a $\text{\TeX}/\text{\LaTeX}$ file prepared by the author.